Front. Environ. Sci. Eng. 2014, 8(6): 825–834
DOI 10.1007/s11783-014-0682-9

RESEARCH ARTICLE

Recovery of NH_4^+ by corn cob produced biochars and its potential application as soil conditioner

Yang ZHANG, Zifu LI (✉), Ibrahim B MAHMOOD

School of Civil & Environmental Engineering, University of Science and Technology Beijing, Beijing 100083, China

Abstract NH_4^+ ion, a main pollutant in aquatic systems, not only causes eutrophication in rivers and lakes but also contributes to fish toxicity. In this study, an eco-friendly biosorbent was prepared from the pyrolysis of corn cob, a low-cost agricultural residue. The biochars produced by pyrolysis of corn cob at 400°C and 600°C were characterized and investigated as adsorbents for NH_4^+-N from an aqueous solution. The biochars were characterized through elemental analysis, Brunauer–Emmett–Teller–N_2 surface area analysis, scanning electron microscopy, and Fourier transform infrared spectroscopy. Batch experiments were conducted to investigate the NH_4^+ adsorption process of the corn cob biochars. The Freundlich isotherm model fitted the adsorption process better than the Langmuir and Dubinin–Radushkevich isotherm models. Moreover, the adsorption process was well described by a pseudo-second-order kinetic model. Results of thermodynamic analysis suggested that adsorption was a nonspontaneous exothermic process. Biochars produced at 400°C had higher adsorption capacity than those produced at 600°C because of the presence of polar functional groups with higher acidity. The exhausted biochar can be potentially used as soil conditioner, which can provide 6.37 kg $NH_4^+-N \cdot t^{-1}$ (N fertilizer per ton of biochar).

Keywords corn cob, biochar, NH_4^+ adsorption, isotherm model, kinetic model

1 Introduction

Urban wastewaters usually contain a considerable amount of NH_4^+, a pollutant that can sharply decrease dissolved oxygen and causes eutrophication in rivers and lakes [1]. Moreover, the discharge limits for NH_4^+ have become stringent because of its toxicity to fish and other aquatic life. Despite its negative effects, NH_4^+ is an essential nutrient for plant growth. Removing NH_4^+ from wastewater is important to control N pollution and to recover N for reuse as fertilizer. NH_4^+ can be removed by conventional methods, such as activated sludge process, precipitation, oxidation, and stripping [2]. However, adsorption is more economically feasible and environmentally friendly than all the methods mentioned above [3]. Many studies on the adsorption of NH_4^+ from aqueous solutions have used mineral materials, such as zeolites and activated carbon (AC) [4], as adsorbents. The relatively high prices of zeolites and AC restrict their practical industrial application. In addition, regeneration of exhausted (postsorption) AC and zeolite adsorbents is difficult.

Biochar is a promising alternative because of its low cost. Moreover, biochar can be produced by pyrolysis, under oxygen-limited conditions, of agricultural residues, which are renewable and available in large amounts. Pyrolytic temperature greatly affects the physical and chemical properties of biochar. Corn (*Zea mays*) cob is a common feedstock that can be used to produce biochar; the annual production of corn is approximately 20 million tons in Northern China [5]. Most corn cobs (CC) are discarded by burning or used as fuel, which not only waste the resources contained in CC, but also leads to air pollution. CCs present great potential for use as raw materials in biochar production.

Studies on plant residue- or agricultural waste-derived biochar for sorbing organic pollutants and heavy metals have revealed that the specific area and polar surface sites of adsorbents are the main factors affecting their removal efficiency [6,7]. Mizuta et al. reported that bamboo biochar made at 900°C had relatively higher nitrate adsorption capacity [8]. In the same trend, Ying et al. showed that sugarcane bagasse biochar has ability to remove phosphate

Received July 15, 2013; accepted February 24, 2014

E-mail: zifulee@aliyun.com

from aqueous solution with the removal rate of 3.1% (with the biochar dosage of 2 g·L^{-1}, and the initial phosphate concentration of 30.8 mg·L^{-1}). They also found that biochar produced from Brazilian pepperwood could sorb ammonium ions with the removal rate ranged 3.8%–15.7% (with the biochar dosage of 2 g·L^{-1}, and the initial ammonium concentration of 10 mg·L^{-1}) [9]. However, information on NH_4^+ ion sorption and the associated mechanisms is lacking. Several studies have elucidated potential adsorption mechanisms, including physisorption and chemisorption, for ammonia (gas) on ACs and graphite oxides [10,11]. In addition, NH_4^+ can bind on the surface of the biochar by electrostatic exchange with other cationic species [12]. However, information on the effects of different biochars on NH_4^+ adsorption processes; related mechanisms (including kinetics and thermodynamics), and research on its role as soil conditioner, is still lacking.

This study aims to determine whether or not biochar can be used as an adsorbent to recover NH_4^+-N from an aqueous solution. Two biochars derived from CC at different pyrolytic temperatures (400°C and 600°C) were used to elucidate the mechanisms underlying NH_4^+-N recovery at different temperatures and solid-to-liquid ratios. The potential use of the exhausted biochars as a soil conditioner was also analyzed.

2 Materials and methods

2.1 Biochar preparation

CCs were collected from a farmland in a suburb of Beijing, China. The cobs were air-dried at room temperature, ground, and then passed through a 1 mm sieve. The ground cobs were placed in ceramic crucibles, each covered with a fitting lid, and then pyrolyzed under oxygen-limited conditions in a muffle furnace at different temperatures (i.e., 400°C and 600°C) for 2 h. The biochars were milled to pass through a 0.1 mm sieve for subsequent demineralization with HCl (2 mol·L^{-1}). After centrifugation of the suspensions, the residues were washed with deionized distilled water until the aqueous phase was nearly neutral. The biochars were then dried overnight at 80°C for further use [13]. The biochar samples produced at 400°C and 600°C pyrolytic temperature are hereafter referred to as CC-400 and CC-600, respectively.

2.2 Biochar characterization

The C, H, and N contents of the biochars were determined using a Vario EI Elemental Analyzer (Elementar Company, Germany). Ash content was determined by heating the biochars at 750°C for 4 h. The oxygen content was calculated by mass difference (100% – C, H, N, and ash %). Brunauer–Emmett–Teller (BET) surface areas were determined from N_2 isotherms at 77K using a gas sorption analyzer (NOVA4200e surface area analyzer; Quantachrome instruments, USA). The surface chemistry of the biochar was provided by a Nexus 670 Fourier transform infrared spectroscopy (FTIR) spectrophotometer (Thermo Nicolet Corporation, USA). The spectrum scope was recorded from 4000 cm^{-1} to 400 cm^{-1} with a resolution of 4 cm^{-1}. The surface morphology of the biochars was analyzed under a field-emission scanning electron microscope (FESEM, EVO 18, ZEISS, Germany). The oxygenated acidic surface groups of the biochar samples were determined using Boehm's titration method [14].

2.3 NH_4^+ adsorption experiments

NH_4^+ adsorption experiments were performed using a batch equilibration technique. A stock solution (1000 mg·L^{-1} NH_4^+-N) was prepared by dissolving NH_4Cl in distilled water, and different concentrations were obtained by diluting the stock solution with distilled water. The batch experiments were carried out in stoppered conical flasks containing 50 mL of different initial concentrations of NH_4^+ solutions and adsorbent dose. The samples were placed on a thermostat shaker at a speed of 180 r·min^{-1} at 25°C. After 2 h of agitation, the adsorbent was removed by filtering through a filter paper and then through a 0.45 μm membrane. All tests were performed in triplicate. The amount of NH_4^+-N adsorbed on the biochar was calculated at equilibrium (q_e mg·g^{-1}) and at time t using the following equations:

$$q_e = (C_0 - C_e) \times \frac{V}{m} \ (\mathrm{mg \cdot g^{-1}}), \tag{1}$$

$$q_t = (C_0 - C_t) \times \frac{V}{m} \ (\mathrm{mg \cdot g^{-1}}), \tag{2}$$

where m is the weight of the biochar. C_0 and C_t are the concentration of NH_4^+-N at initial and at time t. C_e is the concentration of NH_4^+-N at equilibrium.

The kinetics of adsorption was studied to understand the mechanism of adsorption. Pseudo-first-order (Eq. (3)) and pseudo-second-order (Eq. (4)) kinetic models were tested for fit with the experimental data of the NH_4^+ adsorption on the biochars. The models are expressed as follows:

Pseudo-first-order kinetic model:

$$q_t = q_e(1 - e^{-k_1 t}), \tag{3}$$

Pseudo-second-order kinetic model:

$$q_t = \frac{k_2 q_e^2 t}{1 + k_2 q_e t}, \tag{4}$$

where t (min) is the contact time, k_1 (min^{-1}) and k_2 (g·mg^{-1} min^{-1}) are the adsorption rate constants, and q_e

and q_t ($mg \cdot g^{-1}$) represent the adsorbed amount of ion by the adsorbent at equilibrium and time t, respectively.

The limiting step in the adsorption process was determined by predicting the diffusion coefficient using a diffusion-based model. An intraparticle diffusion model is used to describe the adsorption process where the intraparticle diffusion resistance is the rate-determining step [15]. The intraparticle diffusion model is given by

$$q_t = k_i t^{1/2} + C, \tag{5}$$

where q_t ($mg \cdot g^{-1}$) is the absorbed amount of ammonium ion at time t, t (min) is the contact time, and k_i ($mg \cdot g^{-1} \cdot min^{-1/2}$) is the intraparticle diffusion rate constant. C is the intercept, which indicates the thickness of the boundary layer. Large C value indicates greater boundary layer effect.

Adsorption isotherms are currently used for fitting experimental results that are based on different adsorption mechanisms. Some of these isotherms include Freundlich, Langmuir, and Dubinin–Radushkevich (D–R).

The nonlinear form of Freundlich and Langmuir isotherms is as follows:

$$q_e = k_F C_e^n, \tag{6}$$

where q_e is the amount of ammonium adsorbed (mg) by per unit mass of adsorbent (g), k_F and n are Freundlich constants related to adsorption capacity and adsorption intensity, respectively, and C_e is the concentration of ammonium in the equilibrium solution ($mg \cdot L^{-1}$).

$$q_e = \frac{q_{max} K_L C_e}{1 + K_L C_e}, \tag{7}$$

where q_{max} is the maximum adsorption capacity ($mg \cdot g^{-1}$), and K_L is the constant of the Langmuir equation related to the enthalpy of the process.

The linear form of the D–R model is as follows:

$$\ln q_e = \ln q_{max} - \beta\varepsilon^2, \tag{8}$$

where β is the constant of the adsorption energy ($mol^2 \cdot J^{-2}$), and ε is the Polanyi potential, described as

$$\varepsilon = RT \ln\left(1 + \frac{1}{C_e}\right), \tag{9}$$

where R is the gas constant ($J \cdot mol^{-1} K^{-1}$), and T is the temperature (K). The mean adsorption energy E ($kJ \cdot mol^{-1}$) can be calculated from parameter β as follows:

$$E = \frac{1}{(-2\beta)^{1/2}}, \tag{10}$$

Chi-square analysis was applied to estimate the degree of difference (χ^2) between the experimental and isotherm data, and to identify a suitable isotherm model for the adsorption of NH_4^+ on biochars. χ^2 can be calculated as

$$\chi^2 = \sum \frac{(q_e^{exp} - q_e^{cal})^2}{q_e^{cal}}, \tag{11}$$

where q_e^{exp} ($mg \cdot g^{-1}$) is the experimental equilibrium absorbed amount and q_e^{cal} ($mg \cdot g^{-1}$) is the equilibrium absorbed amount that was calculated from the isotherm. Small χ^2 value indicates better-fitting isotherm [16].

The temperature effects were estimated by mixing 0.4 g biochar with 50 mL $NH_4^+ - N$ solution at 100 $mg \cdot L^{-1}$ on a shaker at 25°C, 35°C, and 45°C. The thermodynamics of the adsorption processes were analyzed using the following Eqs [17]:

$$K_e = \frac{q_e}{C_e}, \tag{12}$$

$$\Delta G^0 = -RT \ln K_e, \tag{13}$$

$$\ln K_e = \frac{\Delta S^0}{R} - \frac{\Delta H^0}{RT}, \tag{14}$$

where q_e ($mg \cdot g^{-1}$) is the amount of $NH_4^+ - N$ adsorbed on the biochars from the solution at equilibrium, C_e ($mg \cdot L^{-1}$) is the equilibrium concentration of $NH_4^+ - N$ in the solution, R ($J \cdot mol^{-1} \cdot K^{-1}$) is the gas constant 8.314, T (K) is the absolute temperature, and K_e ($L \cdot g^{-1}$) is the adsorption the distribution coefficient.

Statistical analysis of data was performed by one-way analysis of variance (ANOVA), assuming a confidence level of 95% ($p < 0.05$) for statistical significance. All model parameters were evaluated by nonlinear regression using OriginPro8.5 software.

3 Results and discussion

3.1 Characterization of CC biochars

The physicochemical characteristics of the two biochars are shown in Table 1. The C content increased but the H

Table 1 Physicochemical characteristic of two different biochars

properties	CC-400	CC-600
pH	9.3	10.7
ash/%	3.56	3.15
C/%	79.65	84.35
H/%	3.96	2.41
N/%	0.67	0.76
O/%	12.16	9.33
(O + N)/C	0.13	0.09
O/C	0.115	0.083
acidity /($mmol \cdot g^{-1}$)	0.89	0.23
SA/($m^2 \cdot g^{-1}$)	180.1	212.9

and O contents decreased with increasing pyrolytic temperature. As shown in Table 1, the molar O/C ratio decreased with increasing pyrolytic temperature, suggesting that the surface of CC-600 was less hydrophilic than that of CC-400 [18]. The low ratio of (O + N)/C indicates reduced surface polar functional groups in CC-600. The oxygen-containing functional groups on the biochar surface caused the surface acidity/basicity of the material. The total acidity of CC-400 (0.89 mmol·g^{-1}) was significantly ($p < 0.05$) higher than that of CC-600 (0.23 mmol·g^{-1}), which can be attributed to the partial carbonization of the former CC sample.

The surface area of CC-600 was significantly ($p < 0.05$) higher than that of CC-400. High surface area indicates highly porous structures, especially microporous structures. As shown in Fig. 1(a), CC-600 had more pores than CC-400, which causes the higher BET surface area of the former CC sample. The biochar structures were not homogeneous, and irregular pores with different shapes and sizes were observed.

The FTIR spectra of the biochars (CC-400 and CC-600) and their spectroscopic assignment are shown in Fig. 1(b). For CC-400 and CC-600, the band at 3427 cm^{-1} corresponded to the stretching vibration of hydroxyl groups. The spectra of CC-400 were characterized by four principal bands at wave numbers of 3427, 2927, 1614, and 1437 cm^{-1}. The bands at 2927 and 1614 cm^{-1} were assigned to CH_2 and aromatic C = O ring stretching, respectively, whereas the band at 1437 cm^{-1} was assigned to COOH and CHO [19]. However, the band intensities at 3400 cm^{-1} (–OH) and 1614 cm^{-1} (C = O) were dramatically decreased as the pyrolytic temperature increased to 600°C. Moreover, the COOH and phenolic–OH peaks were completely eliminated.

3.2 Effect of contact time and adsorption kinetics

Approximately 50 mL of 100 mg·L^{-1} NH_4^+–N solution was shaken with 0.5 g biochars at 25°C to determine the time required for the biochars to reach equilibrium. The equilibrium studies were performed at selected time intervals ranging from 5 to 240 min. Figure 2 shows the effect of contact time on the NH_4^+ adsorption and the application of kinetic models to NH_4^+–N adsorption by CC-400 and CC-600.

As shown in Fig. 2, the adsorption of NH_4^+ was rapid during the initial 5 min and then gradually attained equilibrium within 60 min. The rapid adsorption rate ensures high efficiency and cost effectiveness. CC-400 had better adsorption performance for NH_4^+ than CC-600.

The fitted curves and coefficients for the pseudo-first-order, the pseudo-second-order, and the intraparticle diffusion models are presented in Figs. 2(a) and 2(b), respectively. Compared with the first-order model, the pseudo-second-order kinetic model showed a better correlation coefficient for both CC-400 and CC-600 (R^2 = 0.961 and R^2 = 0.993, respectively). The high correlation between the experimental data and the pseudo-second-order kinetic model suggests that the adsorption of NH_4^+ on the biochars is well described by the pseudo-second-order kinetic model. Table 2 contains the lists of the adsorption rate constants associated with pseudo-first-order and pseudo-second-order kinetic models.

The amount of adsorbed NH_4^+–N, q_t (mg·g^{-1}), versus the square root of time for the two biochars are shown in Figs. 2(c) and 2(d). In general, the adsorption process includes three steps: external mass transfer, e.g., boundary layer diffusion; intraparticle diffusion; and saturation. However, in the present study, only two steps were clearly observed (Figs. 2(c) and 2(d)). The first linear region with a high slope signaled a rapid external diffusion stage depicting macro-pore or interparticle diffusion, and the second linear region shows a relatively low slope depicting the intraparticle diffusion effects and the gradual equilibrium stage. These results agree with those of other studies on the adsorption of NH_4^+ on zeolite-like adsorbents [20,21]. In the intraparticle diffusion model, the intraparticle diffusion is considered to be the sole rate-limiting step when q_t versus $t^{1/2}$ plots that passes through the origin. When the plot does not pass through the origin, it indicates some degree of boundary layer control, further suggesting that the intraparticle diffusion is not the only rate-limiting step and that other kinetic models may control the rate of adsorption [3]. In the present study, both plots did not pass through the origin, suggesting that intraparticle diffusion is not the rate-limiting step.

3.3 Adsorption isotherms

The calculated correlation coefficients and isotherm constants are listed in Table 3. The adsorption isotherms are shown in Fig. 3. The Freundlich model (R^2 = 0.996, χ^2 = 0.12 – 0.14) fitted the observations better than the Langmuir (R^2 = 0.953 – 0.982, χ^2 = 0.23 – 0.27) and D–R (R^2 = 0.941 – 0.982, χ^2 = 165 – 158) models. High k_F indicates high affinity to NH_4^+ ions, and $0.1 < n < 1$ indicates favorable adsorption [22].

As shown in Table 3, $n < 1$, suggesting favorable removal conditions. Moreover, the n value of CC-400 was lower than that of CC-600, indicating that the former had a higher affinity for NH_4^+ adsorption. CC-600 has a relatively high surface area, and its surface polar functional groups are lower than those of CC-400. Polar functional groups, such as hydroxyl, phenol, and carboxyl groups, are the main active groups for NH_4^+ adsorption [23]. Biochars can interact with polar groups, such as – COOH, C = O, and/or phenolic–OH, through hydrogen bonding.

A comparison between the FTIR spectra before and after the adsorption of NH_4^+ on the biochars was performed to determine the functional groups involved in the process

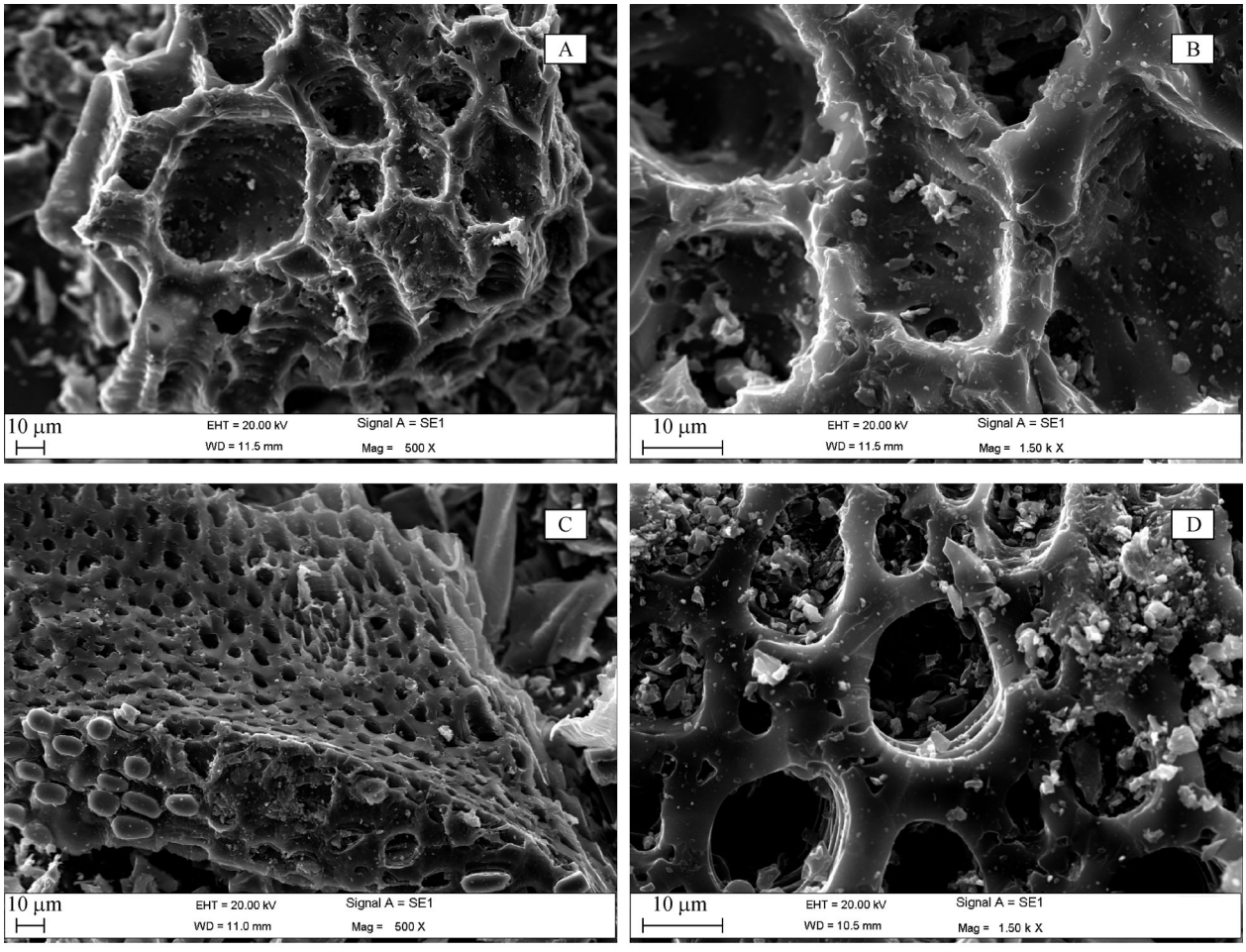

Fig. 1 (a) SEM images of CC-400 (A, B) and CC-600 (C, D); (b) FTIR spectra of CC-400 and CC-600

(supplemental Fig. S-1). The differences are shown in supplemental Table S-1. These differences may be attributed to the changes in counter ions associated with carboxylate and hydroxylate anions, indicating that acidic groups, carboxyl and hydroxyl, are the predominant contributors in the complexation of NH_4^+ ions. In addition, the (O + C)/N ratio of CC-400 was significantly ($p < 0.05$) higher than that of CC-600, suggesting that the former was more hydrophilic than the latter and can easily absorb NH_4^+ ions from the aqueous solution. The mean adsorption

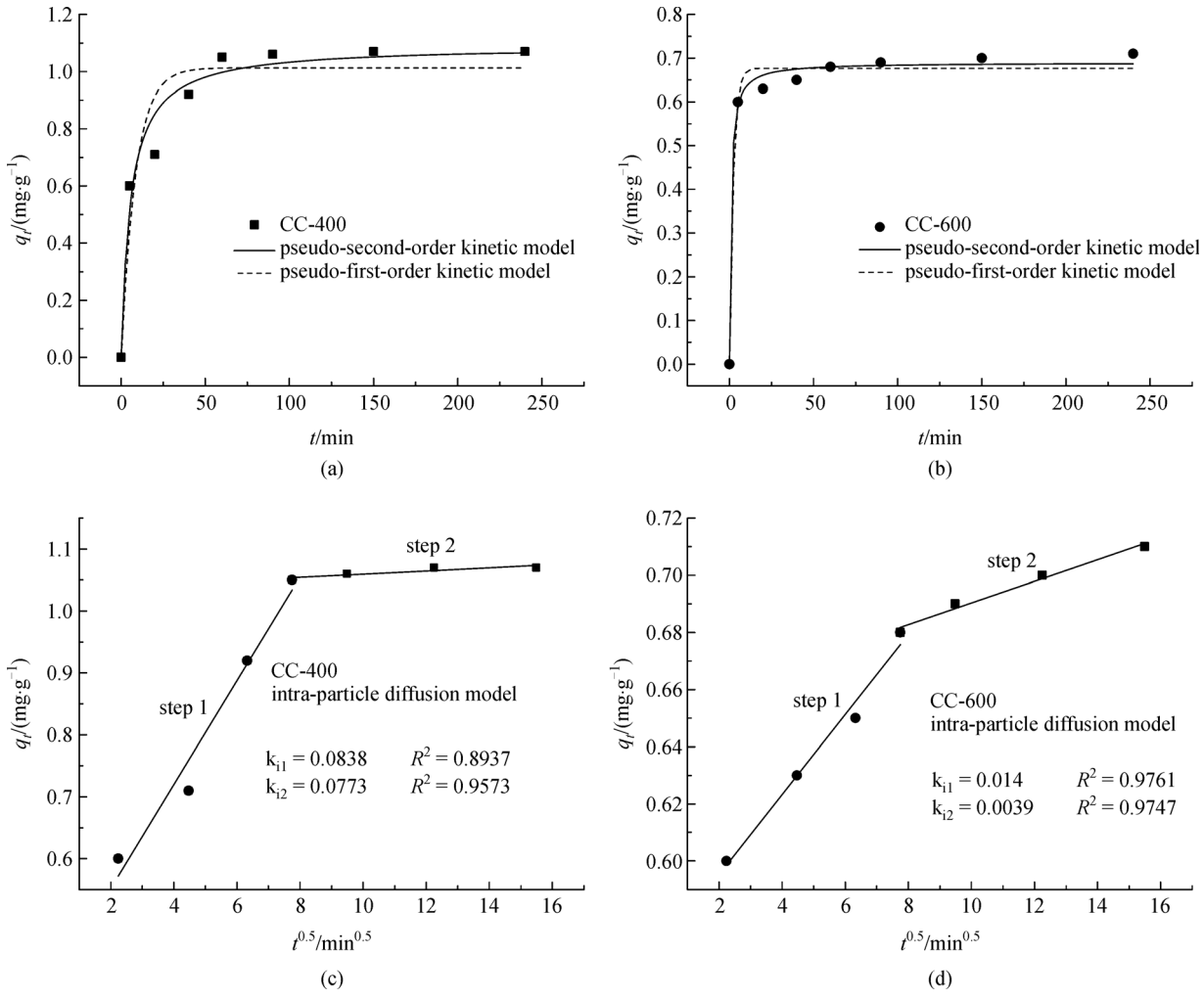

Fig. 2 Application of nonlinear pseudo-first-order and pseudo-second-order kinetic models, and intraparticle diffusion model for NH_4^+ ion adsorption by CC-400 and CC-600: (a) CC-400; (b) CC-600; (c) intraparticle diffusion model for CC-400; (d) intraparticle diffusion model for CC-600

Table 2 Kinetic parameters for ammonium ion adsorption on biochars

kinetic model	parameter	value	
		CC-400	CC-600
pseudo-first-order	k_1 (min^{-1})	0.116	0.435
	q_e (mg·g^{-1})	1.013	0.677
	R^2	0.902	0.986
	SD	0.052	0.011
pseudo-second-order	k_2 (g·mg^{-1}·min^{-1})	0.164	1.675
	q_e (mg·g^{-1})	1.091	0.690
	R^2	0.961	0.993
	SD	0.004	0.001

energy was less than 8 kJ·mol^{-1}, indicating that this adsorption can be dominated by a physical process.

A comparison with previously reported adsorbents for NH_4^+ adsorption is shown in Table 4. As shown in the table, the adsorbed amount of CC-400 is significantly higher than that of *Posidonia oceanica* fibers, natural

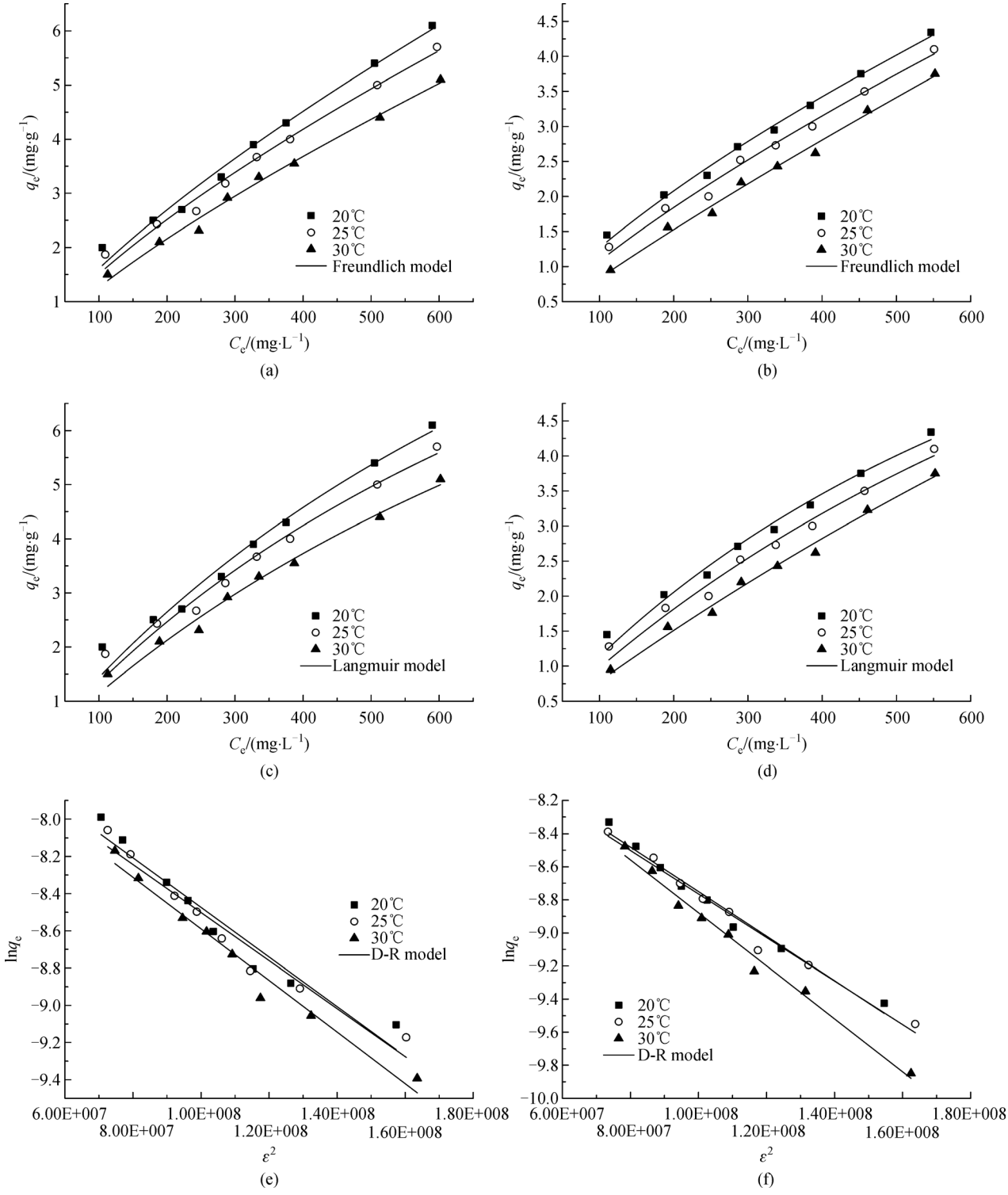

Fig. 3 Nolinear Freundlich and Langmuir isotherms of NH_4^+ sorption on the biochars and Linear D-R isotherm: (a) Freundlich model of CC-400; (b) Freundlich model of CC-600; (c) Langmuir model of CC-400; (d) Langmuir model of CC-600; (e) D–Rmodel of CC-400; (f) D–R model of CC-600

zeolite and hardwood biochar, but lower than that of microwave-treated zeolite. These results suggest that biochars are potential adsorbent materials for the removal of NH_4^+ from aqueous solutions.

Table 3 Constants and correlation coefficient of Langmuir, Freundlich and Dubinin-Radushkevich models for NH_4^+ adsorption onto CC-400 and CC-600

	parameters	CC-400			CC-600		
		20°C	25°C	30°C	20°C	25°C	30°C
Langmuir model	$q_{max}/(mg \cdot g^{-1})$	16.9	15.3	15.3	10.9	12.8	11.5
	$K_L/(L \cdot mg^{-1})$	0.0009	0.0009	0.0008	0.0012	0.0008	0.0003
	R^2	0.973	0.974	0.981	0.953	0.982	0.982
	χ^2	0.23	0.23	0.24	0.25	0.23	0.27
Freundlich model	$k_F()$	0.052	0.051	0.037	0.046	0.030	0.013
	n	0.74	0.73	0.77	0.71	0.77	0.89
	R^2	0.996	0.996	0.996	0.996	0.996	0.996
	χ^2	0.12	0.12	0.13	0.13	0.14	0.13
D-R model	$q_{max}/(mg \cdot g^{-1})$	14.2	13.3	13.4	11.0	10.6	12.4
	$E/(kJ \cdot mol^{-1})$	3.76	3.86	3.60	3.70	3.80	3.10
	R^2	0.941	0.953	0.972	0.982	0.982	0.982
	χ^2	167	167	168	165	167	167

Table 4 Comparison between various adsorbents used for ammonium nitrogen removal

adsorbents	adsorption capacity /$(mg \cdot g^{-1})$	references
Posidonia oceanica fibers	1.73	[24]
natural zeolite	4.04	[25]
hardwood biochar	5.3	[26]
microwave-treated zeolite	23.83	[27]
CC-400	6.37	this study

3.4 Thermodynamic studies

The thermodynamic parameters (ΔH^0, ΔS^0, and ΔG^0) of sorption can be used to define whether or not sorption is endothermic or exothermic. Studies on the effect of temperature on NH_4^+ adsorption showed that NH_4^+ adsorption decreases with increasing temperature.

The thermodynamic parameters for NH_4^+ adsorption on CC-400 and CC-600 were calculated from the linear plot of $\ln K_e$ versus $1/T$. Furthermore, the standard Gibbs free energy (ΔG^0) at each temperature was calculated using Eq. (14). The related figure and parameters are presented in supplemental Fig.S-2 and Table S-2.

As shown in Table S-2, changes in the standard free energy have positive values of 10.4, 11.6, and 13.5 kJ $\cdot mol^{-1}$ for CC-400 and 11.7, 13.2, and 14.8 $kJ \cdot mol^{-1}$ for CC-600 at 283K, 298K, and 313K, respectively. These results indicate that the adsorption might not occur spontaneously. In addition, the factor driving NH_4^+ adsorption to CC-400 and CC-600 remains unclear because the ΔG^0 values were positive. The same phenomenon was observed by Karadag et al. [28], who used natural Turkish clinoptilolite to adsorb NH_4^+ from aqueous solution. The change in the standard enthalpy ΔH^0 yielded negative values of -19.2 and -17.6 $kJ \cdot mol^{-1}$, indicating that NH_4^+ adsorption is an exothermic process. The negative value of the standard entropy change suggests that randomness decreases the removal of NH_4^+ on the biochars.

3.5 Evaluate exhausted biochars as potential soil conditioner

Previous studies have recommended combining biochars with inorganic or organic fertilizers for crop production to significantly improve crop yield. Because the ammonium contained in the traditional fertilizer could be bonded by the biochar and slow-release to the soil, therefore ammonium nitrogen will be sorbed by plants more effectively [29]. However, the optimal amount of an applied biochar varies depending on the soils, crops, and properties of the biochar. Table 5 summarizes the findings of previous experiments involving the application of biochars or biochars with N-fertilizer [30–33].

As shown in Table 5, the application rate of the biochars was 8–100 $t \cdot ha^{-1}$ in the pot and field studies. Moreover,

Table 5 List of the experimental results in some literatures that have applied biochar

location	plants	exp	AP /(t·ha^{-1})	N-fertilizer /(kg·ha^{-1})	effect	references
Australia	Radish	P	10	100	no effect	[30]
Australia	Radish	P	50	100	+ 95%	[30]
Australia	Radish	P	100	100	+ 266%	[30]
Australia	Radish	P	50	100	+ 320%	[31]
Japan	Rice	F	8	50	+ 30%	[32]
China	Maize	F	40	300	+ 12%	[33]

Notes: the column named exp indicates the type of the experiments (F = field study; P = pot); the column named AP and N-fertilizer represent biochar and N-fertilizer application rate, respectively. The column named effect indicates the increased yield production (+ = increment)

combining biochar with N fertilizer can obviously improve crop yield. Thus, the adsorption capacity of the CC biochars is 6.37 mg·g^{-1}, which means that it can provide 6.37 kg $NH_4^+ - N \cdot t^{-1}$ (i.e., N fertilizer per ton of biochar). Normally, N fertilizer is applied between the rate of 80 and 150 kg N·ha^{-1}, however, according to the data provided by the Food and Agriculture Organization, nitrogen utilization efficiency could reach 50%–70% only in a few developed countries. In most developing countries like China, nitrogen utilization efficiency was only 35% [34]. In addition, the application of biochar can reduce the leaching of nutrients (ammonium, potassium and phosphorous ions), thus the sorbed ammonium in the biochar can be utilized more effectively than traditional ammonium nitrogen fertilizer. Lastly, due to the biochar's strong affinity to NH_4^+ and high nutrient retention capacity, the environmental pollution resulting from N volatilization and leakage by the traditional ammonium fertilizer can be reduced. Therefore, exhausted biochars have potential as an eco-friendly technology for improving soil physico-chemical properties and crop productivity.

4 Conclusions

This study investigated the ability of two biochars derived from CC to adsorb $NH_4^+ - N$ from aqueous solution. Kinetic studies showed that the adsorption process was rapid and reached equilibrium within 60 min and that the kinetic data fitted well with the pseudo-second-order kinetic model. The equilibrium NH_4^+ uptake amounts for CC-400 and CC-600 were 1.09 and 0.69 mg·g^{-1}, respectively. The adsorption capacity decreased with increasing adsorbent dosage. Good correlation coefficient values suggest that NH_4^+ adsorption on CC biochars can be best described by the Freundlich adsorption isotherm and that the adsorption process is exothermic. The polar functional groups participate in the adsorption of NH_4^+. These results suggest that CC biochars can be used as adsorbents for NH_4^+. The exhausted biochars can be used as a soil conditioner to improve soil quality and productivity.

Acknowledgements This research was supported by the Fundamental Research Funds for the Central Universities (FRF-IC-11-001).

Supplementary material is available in the online version of this article at http://dx.doi.org/10.1007/s11783-014-0682-9 and is accessible for authorized users.

References

1. Zhang Y, Yan R, Zou Z, Wang J, Rittmann B E. Improved nitrogen removal in dual-contaminated surface water by photocatalysis. Frontiers of Environmental Science & Engineering, 2012, 6(3): 428–436
2. Hung C M, Lou J C, Lin C H. Removal of ammonia solutions used in catalytic wet oxidation processes. Chemosphere, 2003, 52(6): 989–995
3. Ma Z H, Li Q, Yue Q Y, Gao B Y, Li W H, Xu X, Zhong Q Q. Adsorption removal of ammonium and phosphate from water by fertilizer controlled release agent prepared from wheat straw. Chemical Engineering Journal, 2011, 171(3): 1209–1217
4. Vassileva P, Tzvetkova P, Nickolov R. Removal of ammonium ions from aqueous solutions with coal-based activated carbons modified by oxidation. Fuel, 2009, 88(2): 387–390
5. Yan L. Basic study on the comprehensive utilization of the corn cob. Dissertation for the Master Degree. Jilin: Jilin University, 2009 (in Chinese)
6. Chen X, Chen G, Chen L, Chen Y, Lehmann J, McBride M B, Hay A G. Adsorption of copper and zinc by biochars produced from pyrolysis of hardwood and corn straw in aqueous solution. Bioresource Technology, 2011, 102(19): 8877–8884
7. Chen B, Chen Z. Sorption of naphthalene and 1-naphthol by biochars of orange peels with different pyrolytic temperatures. Chemosphere, 2009, 76(1): 127–133
8. Mizuta K, Matsumoto T, Hatate Y, Nishihara K, Nakanishi T. Removal of nitrate-nitrogen from drinking water using bamboo powder charcoal. Bioresource Technology, 2004, 95(3): 255–257
9. Yao Y, Gao B, Zhang M, Inyang M, Zimmerman A R. Effect of biochar amendment on sorption and leaching of nitrate, ammonium, and phosphate in a sandy soil. Chemosphere, 2012, 89(11): 1467–1471
10. Petit C, Kante K, Bandosz T J. The role of sulfur-containing groups in ammonia retention on activated carbons. Carbon, 2010, 48(3):

654–667
11. Seredych M, Petit C, Tamashausky A V, Bandosz T J. Role of graphite precursor in the performance of graphite oxides as ammonia adsorbents. Carbon, 2009, 47(2): 445–456
12. Hale S E, Alling V, Martinsen V, Mulder J, Breedveld G D, Cornelissen G. The sorption and desorption of phosphate-P, ammonium-N and nitrate-N in cacao shell and corn cob biochars. Chemosphere, 2013, 91(11): 1612–1619
13. Zhang G X, Zhang Q, Sun K, Liu X T, Zheng W J, Zhao Y. Sorption of simazine to corn straw biochars prepared at different pyrolytic temperatures. Environmental Pollution, 2011, 159(10): 2594–2601
14. Chun Y, Sheng G, Chiou C T, Xing B. Compositions and sorptive properties of crop residue-derived chars. Environmental Science & Technology, 2004, 38(17): 4649–4655
15. Sureshkumar M K, Das D, Mallia M B, Gupta P C. Adsorption of uranium from aqueous solution using chitosan-tripolyphosphate (CTPP) beads. Journal of Hazardous Materials, 2010, 184(1–3): 65–72
16. Viswanathan N, Meenakshi S. Selective sorption of fluoride using Fe(III) loaded carboxylated chitosan beads. Journal of Fluorine Chemistry, 2008, 129(6): 503–509
17. Sekar M, Sakthi V, Rengaraj S. Kinetics and equilibrium adsorption study of lead(II) onto activated carbon prepared from coconut shell. Journal of Colloid and Interface Science, 2004, 279(2): 307–313
18. Cornelissen G, Gustafsson Ö, Bucheli T D, Jonker M T O, Koelmans A A, van Noort P C M. Extensive sorption of organic compounds to black carbon, coal, and kerogen in sediments and soils: mechanisms and consequences for distribution, bioaccumulation, and biodegradation. Environmental Science & Technology, 2005, 39(18): 6881–6895
19. Wolbach W S, Anders E. Elemental carbon in sediments: determination and isotopic analysis in the presence of kerogen. Geochimica et Cosmochimica Acta, 1989, 53(7): 1637–1647
20. Zhao Y, Yang Y, Yang S, Wang Q, Feng C, Zhang Z. Adsorption of high ammonium nitrogen from wastewater using a novel ceramic adsorbent and the evaluation of the ammonium-adsorbed-ceramic as fertilizer. Journal of Colloid and Interface Science, 2013, 393(0): 264–270
21. Uğurlu M, Karaoğlu M H. Adsorption of ammonium from an aqueous solution by fly ash and sepiolite: isotherm, kinetic and thermodynamic analysis. Microporous and Mesoporous Materials, 2011, 139(1–3): 173–178
22. Raji C, Anirudhan T S. Batch Cr(VI) removal by polyacrylamide-grafted sawdust: kinetics and thermodynamics. Water Research, 1998, 32(12): 3772–3780
23. Liu H, Dong Y, Wang H, Liu Y. Ammonium adsorption from aqueous solutions by strawberry leaf powder: equilibrium, kinetics and effects of coexisting ions. Desalination, 2010, 263(1–3): 70–75
24. Jellali S, Wahab M A, Anane M, Riahi K, Jedidi N. Biosorption characteristics of ammonium from aqueous solutions onto Posidonia oceanica (L.) fibers. Desalination, 2011, 270(1–3): 40–49
25. Liang Z, Ni J. Improving the ammonium ion uptake onto natural zeolite by using an integrated modification process. Journal of Hazardous Materials, 2009, 166(1): 52–60
26. Sarkhot D V, Ghezzehei T A, Berhe A A. Effectiveness of biochar for sorption of ammonium and phosphate from dairy effluent. Journal of Environmental Quality, 2013, 42(5): 1545–1554
27. Lei L, Li X, Zhang X. Ammonium removal from aqueous solutions using microwave-treated natural Chinese zeolite. Separation and Purification Technology, 2008, 58(3): 359–366
28. Karadag D, Koc Y, Turan M, Armagan B. Removal of ammonium ion from aqueous solution using natural Turkish clinoptilolite. Journal of Hazardous Materials, 2006, 136(3): 604–609
29. Steiner C, Teixeira W, Lehmann J, Nehls T, Macêdo J, Blum W H, Zech W. Long term effects of manure, charcoal and mineral fertilization on crop production and fertility on a highly weathered Central Amazonian upland soil. Plant and Soil, 2007, 291(1–2): 275–290
30. Chan K Y, Van Zwieten L, Meszaros I, Downie A, Joseph S. Agronomic values of greenwaste biochar as a soil amendment. Soil Research (Collingwood, Vic.), 2007, 45(8): 629–634
31. Chan K Y, Van Zwieten L, Meszaros I, Downie A, Joseph S. Using poultry litter biochars as soil amendments. Soil Research (Collingwood, Vic.), 2008, 46(5): 437–444
32. Asai H, Samson B K, Stephan H M, Songyikhangsuthor K, Homma K, Kiyono Y, Inoue Y, Shiraiwa T, Horie T. Biochar amendment techniques for upland rice production in Northern Laos: 1. soil physical properties, leaf SPAD and grain yield. Field Crops Research, 2009, 111(1–2): 81–84
33. Zhang A F, Liu Y M, Pan G X, Hussain Q, Li L Q, Zheng J W, Zhang X H. Effect of biochar amendment on maize yield and greenhouse gas emissions from a soil organic carbon poor calcareous loamy soil from Central China Plain. Plant and Soil, 2012, 351(1–2): 263–275
34. Zhang W L, Wu S X, Ji H J, Kolbe H. Estimation of agricultural non-point source pollution in China and the alleviating strategies. Scientia Agricultura Sinica, 2004, 37(07): 1008–1017 (in Chinese)